nature plants

Article

https://doi.org/10.1038/s41477-022-01278-9

Seasonal peak photosynthesis is hindered by late canopy development in northern ecosystems

Received: 26 March 2022

Accepted: 18 October 2022

Published online: 08 December 2022

Check for updates

Qian Zhao[1], Zaichun Zhu[2,3] ✉, Hui Zeng[2,3], Ranga B. Myneni[4], Yao Zhang[1], Josep Peñuelas[5,6] & Shilong Piao[1,7] ✉

The seasonal dynamics of the vegetation canopy strongly regulate the surface energy balance and terrestrial carbon fluxes, providing feedbacks to climate change. Whether the seasonal timing of maximum canopy structure was optimized to achieve a maximum photosynthetic carbon uptake is still not clear due to the complex interactions between abiotic and biotic factors. We used two solar-induced chlorophyll fluorescence datasets as proxies for photosynthesis and the normalized difference vegetation index and leaf area index products derived from the moderate resolution imaging spectroradiometer as proxies for canopy structure, to characterize the connection between their seasonal peak timings from 2000 to 2018. We found that the seasonal peak was earlier for photosynthesis than for canopy structure in >87.5% of the northern vegetated area, probably leading to a suboptimal maximum seasonal photosynthesis. This mismatch in peak timing significantly increased during the study period, mainly due to the increasing atmospheric CO_2, and its spatial variation was mainly explained by climatic variables (43.7%) and nutrient limitations (29.6%). State-of-the-art ecosystem models overestimated this mismatch in peak timing by simulating a delayed seasonal peak of canopy development. These results highlight the importance of incorporating the mechanisms of vegetation canopy dynamics to accurately predict the maximum potential terrestrial uptake of carbon under global environmental change.

The seasonal characteristics of terrestrial vegetation strongly regulate the global carbon (C) cycle[1,2]. Changes in growing-season length (GSL) and maximum seasonal photosynthesis well explain the interannual variations of gross primary production (GPP) but maximum seasonal photosynthesis (GPP_{max}) accounts for more of the interannual changes in GPP than does GSL[3]. Understanding the underlying mechanisms that determine GPP_{max} is therefore critical[4]. Evidence suggests an enhancement of the peak growth of global natural vegetation due to environmental changes[5] and a widespread advance in the timing of the seasonal peak photosynthetic activity across the north caused by warming[6].

[1]Institute of Carbon Neutrality, Sino-French Institute for Earth System Science, College of Urban and Environmental Sciences, Peking University, Beijing, China. [2]School of Urban Planning and Design, Shenzhen Graduate School, Peking University, Shenzhen, China. [3]State Key Laboratory of Tibetan Plateau Earth System, Resources and Environment (TPESRE), Institute of Tibetan Plateau Research, Chinese Academy of Sciences, Beijing, China. [4]Key Laboratory of Earth Surface System and Human—Earth Relations, Ministry of Natural Resources of China, Shenzhen Graduate School, Peking University, Shenzhen, China. [5]Department of Earth and Environment, Boston University, Boston, MA, USA. [6]CSIC, Global Ecology Unit CREAF-CSIC-UAB, Barcelona, Catalonia, Spain. [7]CREAF, Barcelona, Catalonia, Spain. ✉e-mail: zhu.zaichun@pku.edu.cn; slpiao@pku.edu.cn

 https://doi.org/10.1038/s41477-022-01278-9

GPP_{max} is jointly controlled by canopy structure and light-use efficiency (LUE) which are regulated by environmental conditions and the biochemical characteristics of the vegetation[7–10]. The synchrony between the seasonal development of canopy structure and resource availability determines the magnitude of GPP_{max} and the potential maximum GPP_{max} would only be achieved when the densest canopy can match the highest resource availability[7,10]. In this case, the timing (day of the year, DOY) of GPP_{max} (DOY_{GPP}) would be close to the timing of seasonal peak canopy structure (DOY_{CAN}), that is, synchrony between DOY_{GPP} and DOY_{CAN}. However, whether plants can mediate the seasonal development of canopy structure to match the seasonal optimal resource availability to maximize GPP_{max} is unclear, especially under the dramatic global environmental changes. The lack of an indepth understanding of the underlying mechanisms controlling the synchrony between DOY_{GPP} and DOY_{CAN} and its impact on GPP_{max} constitutes a significant uncertainty in understanding the plant's regulation mechanisms and ecosystem carbon uptake capacity under future climate change.

Here, we investigated the synchrony of seasonal peak timing between photosynthesis and canopy structure in northern ecosystems (>30° N) and its influencing factors during 2000–2018 based on satellite observations and flux-tower measurements. We quantified the difference between DOY_{GPP} and DOY_{CAN} ($\delta DOY_{GPP,CAN}$) using two solar-induced chlorophyll fluorescence (SIF) satellite datasets (spatially contiguous SIF (CSIF[11]) and SIF from the Global Ozone Monitoring Experiment-2 (GOME-2 SIF[12]) as proxies for vegetation photosynthesis) and two vegetation indices (normalized difference vegetation index (NDVI) from the moderate resolution imaging spectroradiometer (MODIS) and gap-filled MODIS leaf area index (LAI)[13] as proxies for canopy structure). The factors driving the spatiotemporal variation in the difference between DOY_{CSIF} and DOY_{NDVI} ($\delta DOY_{CSIF,NDVI}$) were investigated on the basis of the boosted regression tree model (BRT)[14] that incorporated a set of biotic and abiotic factors. An optimal GPP_{max} conceptual model was built to investigate the potential of ecosystem GPP_{max} using flux-tower data (Methods). The performance of an ensemble of 14 state-of-the-art ecosystem models in reproducing the observed difference between DOY_{GPP} and DOY_{CAN} was also evaluated.

Results and discussion

Seasonal peak timing and potential climatic constraints

We first analysed the seasonal peak timing differences between vegetation photosynthesis, canopy structure and climatic variables. Soil-water content (SWC) peaked across northern vegetated land in May (DOY_{SWC} = 134), followed by solar radiation (Rad) and temperature (TEMP) in June (DOY_{Rad} = 172) and July (DOY_{TEMP} = 202) respectively. Vegetation generally reaches its annual maximum photosynthesis and canopy structure in July, which is closer to the timing of the seasonal peak temperature compared to SWC and Rad. The timings of peak seasonal photosynthesis and canopy structure were mismatched, with the former peaking 8 days earlier than the latter (DOY_{CSIF} = 188 versus DOY_{NDVI} = 196) (Fig. 1a). The spatial patterns of DOY_{CSIF} and DOY_{NDVI} were nevertheless similar. Photosynthesis and canopy structure peaked around July and August at high northern latitudes and in southern China, closer to the timing of the seasonal peak of temperature, and in other temperate regions they peaked much earlier, closer to the timing of the seasonal peak of SWC (Fig. 1b–f). The spatial patterns of DOY_{GPP} and DOY_{CAN} derived from CSIF and NDVI were corroborated by the independent GOME-2 SIF and gap-filled MODIS LAI (Supplementary Fig. 1).

Photosynthesis peaked earlier than canopy structure in >87.5% of the northern vegetated area (average negative $\delta DOY_{CSIF,NDVI}$ = −10 d) (Fig. 2a). The widespread negative $\delta DOY_{CSIF,NDVI}$ suggested that the vegetation at most northern latitudes did not allocate sufficient C to leaves to form the maximum canopy structure until the seasonal photosynthetic peak. In contrast, 12.3% of northern vegetation (mainly in midwestern Eurasia, parts of China and midwestern North America) had a positive $\delta DOY_{CSIF,NDVI}$ (average positive $\delta DOY_{CSIF,NDVI}$ = 5 d), indicating a strategy prioritizing the allocation of C to leaves. This difference between DOY_{GPP} and DOY_{CAN} was consistent with a previous study[15] and was also supported by GOME-2 SIF and gap-filled MODIS LAI (Extended Data Fig. 1). We also examined the climatic constraints on the timing of seasonal peak photosynthesis across northern ecosystems based on the positioning of DOY_{CSIF} with respect to the peak timing of climatic factors[6] (Methods). We found that seasonal temperature played a critical role across >75.9% of vegetated areas in northern ecosystems and water availability was the dominant factor for other regions (Fig. 2b). Interestingly, the geographical distributions of $\delta DOY_{CSIF,NDVI}$ and the dominant climatic constraint were strongly correlated. The temperature constraint was spatially consistent with a negative $\delta DOY_{CSIF,NDVI}$ and the water constraint was correlated with a positive $\delta DOY_{CSIF,NDVI}$, indicating the impacts of climatic regulation on the mismatch between DOY_{GPP} and DOY_{CAN}. In other words, climatic factors seem to influence the strategy of seasonal allocation of photosynthetic C to the canopy in the northern lands.

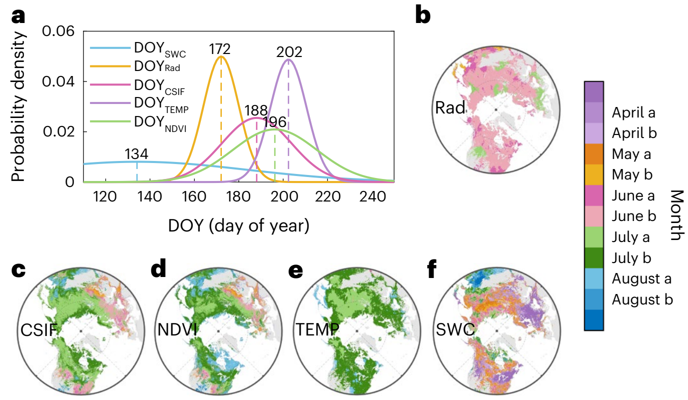

Fig. 1 | Timings of seasonal peak photosynthesis, canopy structure and climatic variables. a, Probability densities of DOY_{CSIF}, DOY_{NDVI}, DOY_{SWC}, DOY_{Rad} and DOY_{TEMP} in northern ecosystems. The dotted lines and numbers indicate their averages weighted by area and CSIF value at the pixel level. **b**–**f**, Spatial patterns of DOY_{Rad}, DOY_{CSIF}, DOY_{NDVI}, DOY_{TEMP} and DOY_{SWC} in northern ecosystems. The legend shows the month of peak timing, with 'a' and 'b' indicating the first half and second half of the month, respectively.

Drivers of the negative $\delta DOY_{CSIF,NDVI}$

Canopy development often consumes only a fraction of photosynthate[16]. Plants usually have the ability to develop the densest canopy to match the highest seasonal resources availability through prioritizing the seasonal allocation of photosynthetic C to canopy. However, why the plants across most of the northern lands failed to do so is unknown. We therefore further investigated the underlying mechanisms of the prevalent earlier peak timing of seasonal photosynthesis than canopy structure (negative $\delta DOY_{CSIF,NDVI}$). To do so, we trained BRT models to examine the influence of 18 biotic and abiotic factors on the negative $\delta DOY_{CSIF,NDVI}$. These factors are closely associated with photosynthesis and the allocation of photosynthates, including climatic factors (climatic conditions and synergies), foliar economic traits, hydraulic traits, indices of biodiversity and other related factors (Methods). The difference between DOY_{GPP} and DOY_{CAN} differed across vegetation types (Extended Data Fig. 2), so we developed separate BRT models for northern ecosystems (entire study area), forests, shrublands and grasslands. The BRT models performed reasonably well (R^2 ranging from 0.69 to 0.91) in explaining the spatial variations of negative $\delta DOY_{CSIF,NDVI}$ (Supplementary Fig. 2).

Climatic factors and foliar economic traits accounted for large fractions of the spatial variation in negative $\delta DOY_{CSIF,NDVI}$ in northern ecosystems and the other three plant types (25.3–46.2% for climatic

https://doi.org/10.1038/s41477-022-01278-9

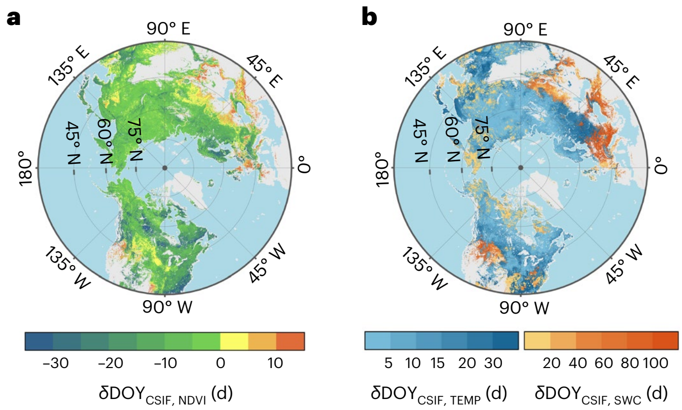

Fig. 2 | Comparison between the timings of seasonal peak photosynthesis and canopy structure in northern ecosystems. a, Spatial pattern of the seasonal peak timing difference between photosynthesis and canopy structure represented by $\delta DOY_{CSIF,NDVI}$ (DOY_{CSIF} − DOY_{NDVI}). **b**, Climatic constraints of temperature (blue) and soil-water content (orange) on vegetation photosynthesis in northern ecosystems, represented by absolute $\delta DOY_{CSIF,TEMP}$ (DOY_{CSIF} − DOY_{TEMP}) and $\delta DOY_{CSIF,SWC}$ (DOY_{CSIF} − DOY_{SWC}), respectively. The absolute values indicate the degree of climatic constraints. Blue or orange color of each pixel represents the dominant limiting factor, temperature or soil-water content, respectively.

conditions, 14.3–19.3% for climatic synergy and 17.9–35.7% for foliar economic traits) (Fig. 3). Climatic factors strongly influenced the peak timings of seasonal photosynthesis and canopy structure in three ways: supplying solar radiation, regulating LUE and determining the strategy for allocating photosynthates. An obvious limitation of light was first detected at high northern latitudes, with a relative contribution of radiation of 22.6% in shrublands (Rad 15.7% and $\delta DOY_{CSIF,Rad}$ 6.9%). We emphasize that a decrease in radiation after summer solstice may not support ongoing vegetation photosynthesis and may therefore alter the seasonal synergy between photosynthesis and canopy structure, consistent with a recent study reporting a limitation of light on autumnal photosynthesis[17]. LUE is sensitive to environmental conditions, as predicted by many LUE models[18]. Climatic synergistic variables would have obvious relative contributions if climatic factors significantly accounted for the negative $\delta DOY_{CSIF,NDVI}$ by inhibiting LUE. However, this was not supported due to the low contributions of $\delta DOY_{CSIF,TEMP}$ and $\delta DOY_{CSIF,SWC}$. The apparent contribution of temperature in forests (TEMP 12.0%) and shrublands (TEMP 7.1%) could therefore be partly attributed to its influence on adaptive strategies of allocating photosynthates. Previous studies have reported that low temperatures could increase the proportion of new C allocated to roots in forests[16,19], leading to a later seasonal peak of canopy structure than photosynthesis. We nonetheless cannot exclude the possibility that climatic factors contributed to the negative $\delta DOY_{CSIF,NDVI}$ through other physiological processes, even though their influences may not have been as strong as those mentioned above.

Foliar economic traits are closely associated with plant photosynthetic capacity, representing plant nutritional status and amount of foliage[20]. Nitrogen concentration per unit dry mass (Nm), phosphorus concentration per unit dry mass (Pm) and specific leaf area (SLA) were used to account for foliar economic traits. Pm was the primary factor driving the spatial variation in negative $\delta DOY_{CSIF,NDVI}$, explaining 20.1% and 15.2% of the variation for forests and northern ecosystems, respectively (Fig. 3). Nutrient limitations have two main physiological impacts on plant growth: primarily limiting the development of leaf area and secondarily regulating photosynthesis[21]. Foliar phosphorus (P) concentration plays a more important role than nitrogen (N) concentration in limiting the development of leaf area[21,22] but foliar N concentration has a stronger and more direct influence than P concentration in regulating photosynthesis[23,24]. Our results emphasize a larger contribution of foliar P concentration than N concentration (Pm 15.2% versus Nm 5.6% for northern ecosystems), suggesting that foliar properties may contribute to negative $\delta DOY_{CSIF,NDVI}$ primarily by delaying canopy development. Delayed canopy structure cannot develop in parallel with the maximum photosynthetic activity. Nm also did not significantly contribute at high northern latitudes (Nm 2.2% for shrublands), even though widespread N limitation has been reported[25,26], implying that the effects of nutrient limitations on photosynthetic capacity were not responsible for the seasonal mismatch between photosynthesis and canopy structure.

As a structural component of genetic material, P strongly controls cell division and the synthesis of enzymes. Experimental studies have reported that plants reduce the growth of biomass before stored P is depleted[27]. Stoichiometry, however, cannot easily set a threshold of P concentration because the growth of biomass declines before P becomes limited[23]. Recent studies have paid more attention to N limitation in northern ecosystems because, as a dominant component of enzymes, N directly influences photosynthetic enzymatic activity[28–30]. Our study emphasizes the neglected effect of P limitation on canopy development at ecosystem scales. This restriction may result in delayed canopy development and seasonal decoupling of photosynthesis and canopy structure and thus influence ecosystem potential maximum photosynthesis, even though it is not linearly connected to photosynthetic activity. The dominant factor driving the spatial variation in negative $\delta DOY_{CSIF,NDVI}$ differs across plant types, partly due to variations in the complexity of canopy structure and environmental conditions (Fig. 3). The seasonal synergy between photosynthesis and canopy structure for forests was primarily controlled by P limitation (Fig. 3a). For shrublands at high northern latitudes, radiation limitation (22.6%) and biodiversity (24.2%) were dominant factors. Biodiversity was a proxy for environmental resources and can reflect the synthesized phenological responses from different species at the ecosystem level[31,32]. The accumulation of C between daytime photosynthesis and night-time consumption by respiration directly determined the seasonality of canopy structure for grasslands, where the diurnal range in temperature (Tdr) was larger than that for other plant types (Tdr 18.3%). In conclusion, the maximum seasonal photosynthesis was generally hindered by late canopy development due to nutrient limitation and climatic regulation in northern ecosystems.

GPP_{max} potential under an optimized $\delta DOY_{GPP,CAN}$

The degree to which GPP_{max} would be enhanced if the late development of canopy structure could be adjusted to match the most abundant resources in a strategy of vegetation optimization is another critical question. We therefore idealized the seasonal peak timing of canopy structure using flux-tower data based on an optimal GPP_{max} conceptual model (Methods). The seasonality of canopy structure in this model was regulated to find an optimal peak timing when environmental resources were most abundant and then an optimal GPP_{max} was reconstructed jointly by the optimal canopy structure and the most abundant resources (for conceptual illustration see Extended Data Fig. 3). The difference between optimized and observed GPP_{max} (δGPP_{max}) can be regarded as the potential increase of ecosystem GPP_{max} and the difference between optimized and observed DOY_{NDVI} (δDOY_{NDVI}) indicates the days of mismatch between the timings of the highest availability of resources and seasonal peak canopy structure. Our results indicated that canopy structure peaked later than photosynthesis at >80% of the flux sites (average negative $\delta DOY_{GPP,NDVI}$ = −11 d) and later than the peak of environmental resources (average negative δDOY_{NDVI} = −19 d), implying that more resources would be obtained with an advanced peak timing of canopy structure (Fig. 4). A larger asynchrony between seasonal peak timings of photosynthesis and canopy structure ($\delta DOY_{GPP,NDVI}$) generally indicated a larger potential increase of GPP_{max} (R^2 = 0.68) and a more intensive regulation of the peak timing of canopy structure

https://doi.org/10.1038/s41477-022-01278-9

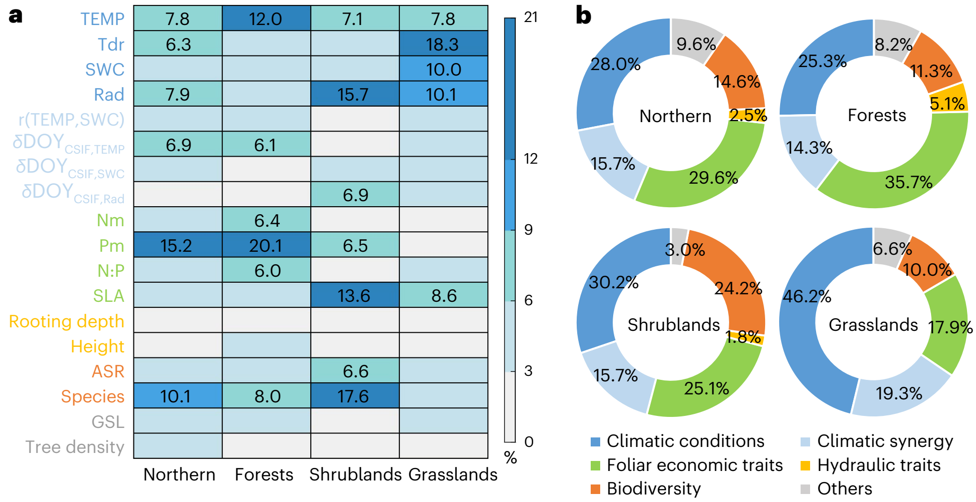

Fig. 3 | Factors accounting for the prevalent earlier seasonal peak timing of photosynthesis than canopy structure. a, Relative contribution of 18 factors influencing the spatial variation of negative $\delta DOY_{CSIF,NDVI}$ evaluated by BRT models for four ecosystems: northern ecosystems, forests, shrublands and grasslands. Different colours of the *y*-axis represent different categories of factors: variables of climatic conditions (TEMP, Tdr, SWC and Rad are dark blue); variables of climatic synergy (*r*(TEMP,SWC), $\delta DOY_{CSIF,TEMP}$, $\delta DOY_{CSIF,SWC}$ and $\delta DOY_{CSIF,Rad}$ are light blue); foliar economic traits (Nm, Pm, N:P and SLA are green); hydraulic traits (rooting depth and canopy height are yellow); biodiversity variables (ASR and species are orange); and others (GSL and tree density are grey) (Methods). **b**, Statistics for the cumulative contribution of the factors from the same category. The colours of the donut chart correspond to the colours of the *y*-axis in **a**.

(δDOY_{NDVI}). We emphasize that a potential increase of GPP_{max} (average δGPP_{max} = 0.17 g C m^{-2} d^{-1}) would be achieved by advancing the seasonal peak timing of canopy structure. These results at the site level imply that the prevalent earlier peak timing of seasonal photosynthesis than of canopy structure at northern latitudes probably led to suboptimal maximum seasonal photosynthesis.

Ecosystem models overestimated $\delta DOY_{GPP,CAN}$

We evaluated the performances of 14 dynamic global vegetation models (DGVMs) that participated in the 'Trends and drivers of the regional scale sources and sinks of carbon dioxide' project (TRENDY v.7) in reproducing the timings of seasonal peak photosynthesis and canopy structure using their GPP and LAI results[33]. The results indicated that all the models overestimated the number of days that vegetation photosynthesis preceded canopy structure ($\delta DOY_{GPP,LAI}$) compared with observations, due to a notably delayed peak timing estimation of canopy structure (DOY_{LAI}) (Fig. 5 and Supplementary Figs. 3 and 4). Benefiting from the mechanistic understanding of photosynthetic processes and the unified photosynthesis module, that is, Farquhar model or its variants[34], the DGVMs simulated a reasonable peak timing of photosynthesis (Supplementary Fig. 5). However, the simulation of the seasonal dynamics of canopy structure involved processes that are currently poorly understood and represented, especially the seasonal C allocation mechanisms, resulting in reported systematic bias of modelled seasonal variations in LAI[35,36].

The modules of C allocation in recent DGVMs are mainly developed on the basis of three strategies: (1) allometric relationships between plant organs[37,38], (2) resource limitation on vegetation growth[39] and (3) both allometric relationships and resource limitation[40,41]. We divided the TRENDY models into three groups according to their strategies for C allocation. We found that the models developed on the basis of a single C allocation strategy provided better (but still poor) simulations of the peak timing of canopy structure (DOY_{LAI} from 195 to 230 for allometric relationships and DOY_{LAI} = 213 for resource limitation) compared with observations (DOY_{NDVI} = 196) (Fig. 5). However, models considering both allometric relationships and resource limitation do not improve their performance, simulated notably delayed peak timings of canopy structure (DOY_{LAI} from 221 to 255) and thus overestimated the $\delta DOY_{GPP,CAN}$ ($\delta DOY_{GPP,LAI}$ from −58 to −25 d). Our results emphasized that all the C

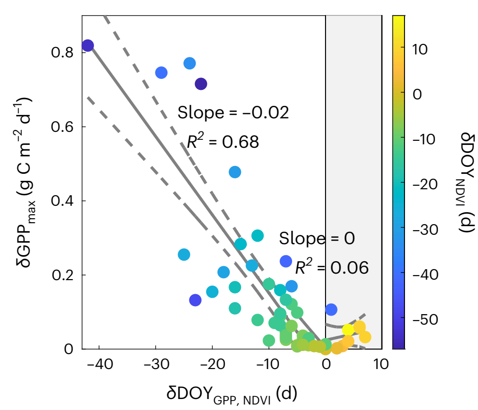

Fig. 4 | Relationship between potential increase of GPP_{max} (δGPP_{max}) and the synchrony of peak timing between canopy structure and photosynthesis ($\delta DOY_{GPP,NDVI}$) at 52 flux-tower sites. Each dot represents a site (n = 52). The colour scale indicates the difference in seasonal peak timing between canopy structure and environmental resources (δDOY_{NDVI}). The solid grey line indicates a linear regression fit and the dashed lines represent the 95% confidence interval.

allocation mechanisms represented in current DGVMs need further improvements and that combining allometric and resource limitation theories without refinement does not improve the performance of the models in simulating seasonal canopy dynamics.

Increasing discrepancy between DOY_{CSIF} and DOY_{NDVI}

Satellite observations suggested that the discrepancy in peak timing between vegetation photosynthesis and canopy structure significantly increased during 2000–2018 (0.39 d per decade, P = 0.04) (Fig. 6a). The overall increasing discrepancy between DOY_{CSIF} and DOY_{NDVI} across the northern lands indicated that the northern vegetation might not be able to tackle the environmental changes and sufficiently alter its seasonal foliar allocation to achieve a larger GPP_{max} (Fig. 6b). The DGVMs from TRENDY project failed to capture the observed trends in the discrepancy between DOY_{CSIF} and DOY_{NDVI}, in terms of both the overall trend (0.32 ± 0.48 d per decade, P = 0.36) and spatial pattern (Fig. 6a,c).

https://doi.org/10.1038/s41477-022-01278-9

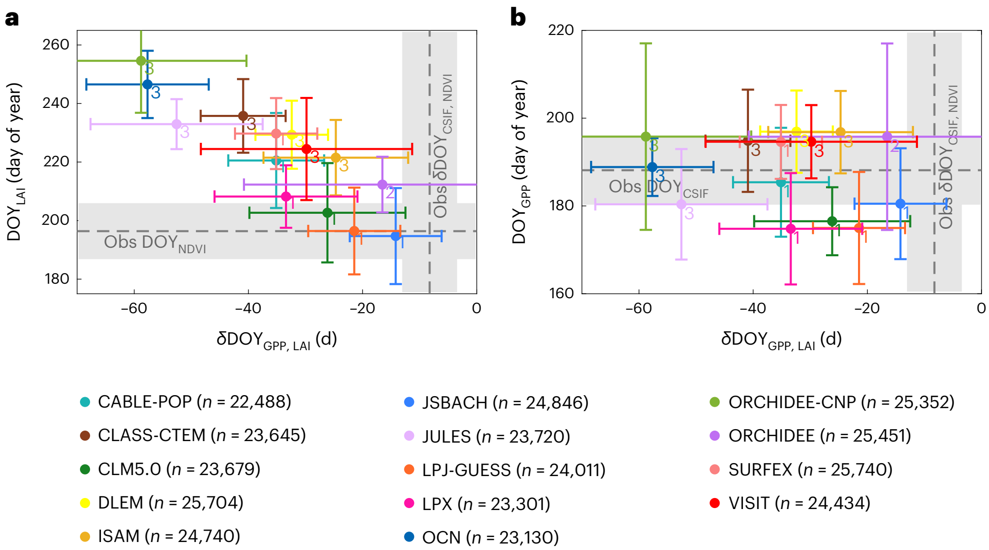

Fig. 5 | Timings of seasonal peak photosynthesis and canopy structure in northern ecosystems simulated by the 14 TRENDY models. a, Comparison of modelled DOY_{LAI} and $\delta DOY_{GPP,LAI}$ with observed DOY_{NDVI} and $\delta DOY_{CSIF,NDVI}$. The coloured dots and error bars represent the spatial means ± 0.5 s.d. among grid cells and the corresponding sample size *n* of each model was also provided. The numerical labels indicate different strategies of allocation of photosynthetic carbon: (1) allometric relationship between plant organs, (2) resource limitation on vegetation growth and (3) both allometric relationships and resource limitation. The grey dotted lines and shading represent the spatial means ± 0.5 s.d. among grid cells of observation (*n* = 25,928). **b**, Same as **a** but for DOY_{GPP} and $\delta DOY_{GPP,LAI}$. Obs, observed.

We further explored the effects of rising atmospheric CO_2 concentration and climate change on the increasing discrepancy between DOY_{CSIF} and DOY_{NDVI} during 2000–2017 based on the BRT model that considers temporal varying atmospheric CO_2 concentration and climate change (Methods). The results indicated that the increasing discrepancy was mainly due to the rising CO_2 (0.46 d per decade) and that it was slightly alleviated by climate change (−0.03 d per decade) (Extended Data Fig. 4). The rising CO_2 amplified the discrepancy between DOY_{CSIF} and DOY_{NDVI} across most of the northern vegetated lands (Extended Data Fig. 4d), probably due to a combined result of earlier DOY_{CSIF} due to the CO_2 fertilization effects on photosynthesis and a relatively stable DOY_{NDVI} that was probably limited by temperature and nutrients and a more conservative carbon allocation strategy[25,42,43]. The increasing CO_2-induced discrepancy suggested that, despite the positive effects of CO_2 fertilization on GPP_{max} (ref. [5]), there was room for further enhancement of GPP_{max} under the assumption that the northern vegetation develop seasonal maximum canopy structure earlier. The effect of climate change on $\delta DOY_{CSIF,NDVI}$ trend was relatively weak compared with rising CO_2 but, interestingly, negative effects of climate change were found in most temperature-limited regions, indicating that warming climate alleviated the discrepancy between DOY_{CSIF} and DOY_{NDVI} during past two decades (Extended Data Fig. 4e). We also explored the contributions of rising CO_2 and climate change to the changes in $\delta DOY_{GPP,LAI}$ based on TRENDY models. The model simulations showed a positive effect of climate change (0.75 ± 0.73 d per decade) and a negative effect of rising CO_2 (−0.10 ± 0.25 d per decade) with large spreads (Supplementary Fig. 6), opposite to the results based on the BRT models. Nevertheless, further studies are needed, especially field experiments designed to investigate the underlying mechanisms controlling $\delta DOY_{GPP,CAN}$, which could provide explicit guidance to further improve the knowledge and implementation of processes and mechanisms that drive the variations in vegetation canopy development in state-of-the-art ecosystem models.

This study used data from multiple sources and analysed the synchrony between the timings of seasonal peak photosynthesis and seasonal peak canopy structure at northern latitudes. Our findings identified a widespread mismatch between the two peak timings and an increasing discrepancy between them, suggesting that northern vegetation could not mediate the seasonal canopy structure to match the availability of resources to maximize its growth, with climatic regulation and nutrient limitation being potential vital reasons.

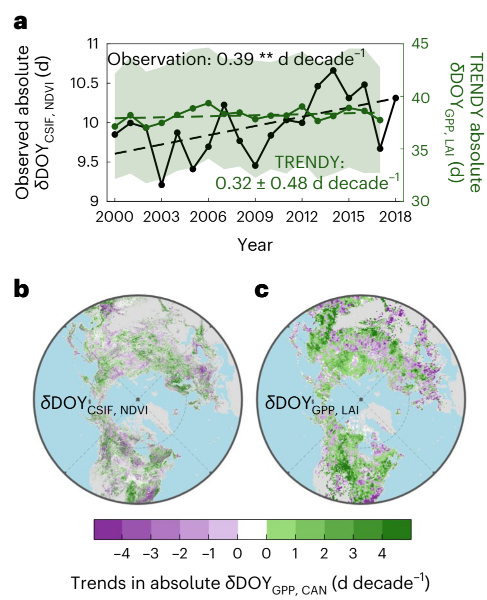

Fig. 6 | Changes in the mismatch in seasonal peak timing between photosynthesis and canopy structure. a, Interannual changes in observed absolute $\delta DOY_{CSIF,NDVI}$ (black lines) and model-simulated absolute $\delta DOY_{GPP,LAI}$ (green lines) obtained by averaging 14 TRENDY models. The solid lines with markers and dotted lines indicate annual mismatched days and regression lines. The trend is calculated by the Theil–Sen estimator and the two-sided significance test is estimated by the Mann–Kendall. Double asterisks indicate significant trend at $P < 0.05$ ($P = 0.04$ for observation and $P = 0.36$ for model simulation). The green shading indicates the uncertainty range represented by the mean value ± 0.5 intermodel standard deviation. **b**,**c**, Spatial patterns of the trends in absolute $\delta DOY_{GPP,CAN}$ derived from observed $\delta DOY_{CSIF,NDVI}$ during 2000–2018 and model-simulated $\delta DOY_{GPP,LAI}$ during 2000–2017. The absolute value of $\delta DOY_{GPP,CAN}$ represents the degree of mismatch in seasonal peak timing between photosynthesis and canopy structure regardless of their relative order.

The current DGVMs generally performed poorly in identifying the observed mismatch in peak timing. Incorporating the findings of this study will provide new insights for improved modelling of seasonal vegetation growth (for example, P cycling and its effects on regulating peak vegetation growth). These mechanisms will help improve our understanding and projection of the maximum potential uptake of C by terrestrial vegetation under dramatic global environmental change.

Methods

Datasets and study area

We used the clear-sky CSIF dataset with 4-day temporal and 0.05° spatial resolutions to derive the annual peak timing of vegetation photosynthesis (DOY_{CSIF}) from 2000 to 2018 in northern ecosystems (>30° N). The CSIF dataset uses surface reflectance from the MODIS Collection 6 (C6) (MCD43C1) as inputs and trains machine-learning algorithms on daily SIF observations from Orbiting Carbon Observatory-2. It was demonstrated to capture well the seasonal dynamics of satellite-observed SIF, which shows high consistency with ecosystem GPP[44–46] and thus CSIF is suitable for vegetation phenology retrievals as a proxy for GPP[11,17]. We used the NDVI dataset from the MODIS C6 (MOD13C1) with 16-day temporal and 0.05° spatial resolutions to retrieve the annual peak timing of vegetation canopy structure (DOY_{NDVI}) from 2000 to 2018. Continuous snow cover leads to abundant missing data at high northern latitudes, so we reconstructed the NDVI time series using an adaptive method of spatiotemporal tensor completion based on the 'pixel reliability' layer from the MOD13C1 dataset to improve the quality of the data[47]. We then interpolated the CSIF and reconstructed NDVI datasets to daily temporal resolution using linear interpolation. Another 16-day NDVI dataset with 500-m spatial resolution from the MODIS C6 (MOD13A1) was also used to extract the seasonality of canopy structure around flux-tower sites.

To test the robustness of the peak timing of photosynthesis derived from CSIF, we used an independent SIF dataset from GOME-2 (ref. [48]). The GOME-2 SIF v.28 product suffered from sensor degradation and large uncertainties due to low signal levels[49] and thus it is not suitable for long-term trend analysis. We therefore derived the peak timing from the multiyear mean seasonal cycle of daily average SIF during 2007–2018. We also used a reprocessed LAI dataset[13] to characterize the peak timing of canopy structure in northern ecosystems to ensure the robustness of our analyses. This LAI data were generated by reprocessing the MODIS C6 LAI product with 8-day temporal and 0.05° spatial resolutions and it performed more continuously and consistently in temporal and spatial domains than MODIS LAI[13], suitable for seasonal peak timing retrievals.

Surface air temperature (TEMP), shortwave radiation (Rad) and SWC were used in this analysis to define the climatic constraints on vegetation photosynthesis in northern ecosystems. TEMP and Rad were obtained from the Climatic Research Unit-National Centers for Environmental Prediction (CRU-NCEP v.9) with 6-hourly temporal and 0.5° spatial resolutions. The SWC dataset was provided by the Global Land Data Assimilation System (GLDAS v.5)[50] with 3-hourly temporal and 0.25° spatial resolutions and we adopted SWC to a depth of 40 cm. These data were aggregated into daily temporal and 0.5° spatial resolutions to derive their annual peak timings (DOY_{TEMP}, DOY_{Rad} and DOY_{SWC}) from 2000 to 2018.

We used the FLUXNET2015 Tier 1 dataset[51] to analyse the potential increase of GPP_{max} based on a conceptual model. We first rigorously selected sites and focused on the sites with only one seasonal GPP peak from spring to autumn (52 sites, Supplementary Table 1). We controlled daily flux data with >75% valid observations and calculated daily GPP as the average of both night-time[52] and daytime[53] partitioning methods. We also compared the GPP estimates of both methods and excluded biased daily GPP to reduce the uncertainty caused by the NEE-partitioning method. The observed seasonal cycles of GPP and Rad were extracted from the daily data with valid fluxes.

The vegetation map was derived from the MODIS C6 (MCD12Q1) with the International Geosphere-Biosphere Programme (IGBP) classification scheme. We only considered vegetated areas >30° N with one peak during the growing season from summer to autumn. Vegetated areas with multiple peaks throughout the year were eliminated using harmonic analysis. We also ignored the vegetated areas with low seasonality based on a threshold of the coefficient of variation of the annual seasonal cycle of NDVI (>0.2).

Retrieval of peak timing

The peak timing was identified as the DOY when the variable arrived at its annual maxima. We retrieved annual peak timings of vegetation photosynthesis (DOY_{CSIF} and DOY_{SIF}), canopy structure (DOY_{NDVI} and DOY_{LAI}) and climatic factors (DOY_{TEMP}, DOY_{Rad} and DOY_{SWC}) from 2000 to 2018. We applied a non-parametric singular spectrum analysis (SSA) to obtain smoothed time series, reduce noise and maintain the seasonal signal of the time series[54]. SSA first decomposes the original time series into oscillatory components and noises with different frequencies based on the singular value decomposition and then reconstructs seasonal signals using the decomposed components. This non-parametric approach can reduce noise components, makes no prior assumptions about the original time series and is widely used to reconstruct time series[6,55].

Definition of climatic constraints

We investigated the impacts of climatic constraints on vegetation photosynthesis in northern ecosystems on the basis of the framework proposed by ref. [6]. This framework is based on two fundamental principles. First, vegetation photosynthesis and radiation will be seasonally consistent without climatic limitations, suggesting that DOY_{CSIF} tends to be equal to DOY_{Rad}. Second, DOY_{CSIF} will tend to be closer to the peak timing of the dominant limiting factor to obtain this more restricted resource than other factors. We adopted the idea of this framework using the peak timings of climatic factors as proxies for resource availability and defined the difference between DOY_{CSIF} and DOY_{TEMP} ($\delta DOY_{CSIF,TEMP}$) and the difference between DOY_{CSIF} and DOY_{SWC} ($\delta DOY_{CSIF,SWC}$) as the temperature and water constraint on vegetation photosynthesis, respectively. The sequential order of the peak timings of climatic factors in northern ecosystems had three scenarios: $DOY_{SWC} < DOY_{Rad} < DOY_{TEMP}$, $DOY_{Rad} < DOY_{SWC} < DOY_{TEMP}$ and $DOY_{Rad} < DOY_{TEMP} < DOY_{SWC}$ (Supplementary Fig. 7). We analysed the climatic constraints on vegetation photosynthesis on the basis of all three scenarios, different from the original framework which only considered the most common scenario in northern ecosystems ($DOY_{SWC} < DOY_{Rad} < DOY_{TEMP}$).

Spatial analysis

We retrieved the seasonal peak timings of photosynthesis, canopy structure and climatic variables and analysed their multiyear average differences from 2000 to 2018 (Fig. 1). We then quantified the mismatch in peak timing between photosynthesis and canopy structure ($\delta DOY_{CSIF,NDVI}$) and examined the climatic constraints on the peak timing of photosynthesis across northern ecosystems (Fig. 2).

We used the BRT model to quantify the relative contributions of 18 extrinsic and intrinsic factors to the spatial variation in negative $DOY_{CSIF,NDVI}$. The BRT model is a machine-learning method based on the regression tree and boosting method, which can accommodate missing data and handle complex interactive effects between predictors. We developed four BRT models dependent on plant type (northern ecosystems, forests, shrublands and grasslands). The BRT models were established on the basis of the 'gbm' R package and defined with a tree complexity of 5, a bag fraction of 0.5 and a learning rate of 0.001 or 0.01 based on the sample size of the response factor. All numeric variables were standardized (z-scores) and the response variable satisfied the assumption of normality in the BRT models. Other analysis and figure generation for this study were performed in MATLAB (R2019b).

Eighteen variables were used as explanatory factors in the BRT models, including: climatic factors—TEMP, SWC, Rad and Tdr for climatic conditions and correlation coefficient between TEMP and SWC (r(TEMP, SWC)), $\delta DOY_{CSIF,TEMP}$, $\delta DOY_{CSIF,SWC}$ and $\delta DOY_{CSIF,Rad}$ for climatic synergies; foliar economic traits—Nm, Pm, the ratio of Nm to Pm (N:P) and SLA; hydraulic traits—maximum rooting depth (rooting depth) and canopy height (height); indices of biodiversity—anthropogenic species richness (ASR) and plant species (species); and other related factors—GSL and tree density (Supplementary Table 2). Climatic factors were divided into two subcategories—climatic conditions and climatic synergies—to emphasize the effects of different processes on the peak timing of seasonal vegetation. Although these explanatory variables may be partially correlated, the BRT model makes no assumptions about variable interactions and can handle the interactions between the explanatory variables[14].

TEMP, SWC and Rad were averaged from 2000 to 2018. Tdr was obtained from NCEP v.9 and averaged during the growing season of the study period to determine their effect on vegetation growth. We took foliar economic traits and hydraulic traits into account because they are closely associated with vegetation photosynthetic capacity and the dynamics of water transport, respectively. Foliar economic traits include Nm, Pm, N:P and SLA, derived from the trait maps based on the TRY database[56] (https://www.try-db.org/TryWeb/Home.php). Hydraulic traits contain maximum rooting depth and canopy height obtained from the Global Earth Observation project for Integrated Water Resource Assessment and the Global 1 km Forest Canopy Height dataset[57]. We also adopted variables of biodiversity in the BRT models, including ASR and plant species because biodiversity and ecosystem functions and processes, such as terrestrial C storage and productivity, are strongly correlated. ASR was developed by ref. [58] using a set of global models and estimates of anthropogenic species gains and losses. Data for plant species were obtained from the dataset Number of Plant Species by Terrestrial Ecoregion developed by ref. [59]. We aggregated all the variables into a common spatial resolution of 0.5°.

Optimal GPP_{max} conceptual model

To explore the potential increase in GPP_{max} of the northern ecosystems, we built an optimal GPP_{max} conceptual model based on flux-tower data and model framework of LUE and the fraction of absorbed photosynthetically active radiation (FAPAR) (equation (1)). In this model, the seasonality of photosynthesis was partitioned into two sections: development of canopy structure and availability of environmental resources. An optimized GPP_{max} would be achieved if plants could regulate their peak timing of seasonal canopy structure (DOY_{NDVI}) to match the timing of the highest availability of resources in a year ($DOY_{Resources}$). We therefore first derived the dynamic of availability of environmental resources from the seasonality of photosynthesis by integrating equations (1)–(3).

$$\mathrm{LUE}_{(t)} = \frac{\mathrm{GPP}_{(t)}}{\mathrm{PAR}_{(t)} \times \mathrm{FAPAR}_{(t)}} \tag{1}$$

GPP was obtained from eddy-covariance flux data, representing the seasonality of photosynthesis. Photosynthetically active radiation (PAR) can be regarded as an extrinsic resource and calculated as the product of observed Rad from the flux tower and a coefficient (set to be 0.45). FAPAR was directly related to the development of canopy structure and estimated as a linear function of NDVI, which was obtained from the MOD13A1 dataset within a radius of the flux-tower site (1 km for forests and 200 m for grasslands and shrublands). LUE can therefore be estimated on the basis of equation (1) and *t* represents the day number of the year.

$$\mathrm{LUE}_{(t)} = \mathrm{HTN}_{(t)} \times \mathrm{Leaf\ Age}_{(t)} \tag{2}$$

LUE is jointly controlled by hydrothermal and nutrient conditions (HTN) and leaf phenology (Leaf Age), closely related to environmental resources and canopy structure. In equation (2), Leaf Age was quantified as a linear function of NDVI[60] and HTN can therefore be estimated.

$$\mathrm{PAR}_{(t)} \times \mathrm{HTN}_{(t)} = \frac{\mathrm{GPP}_{(t)}}{\mathrm{FAPAR}_{(t)} \times \mathrm{Leaf\ Age}_{(t)}} \tag{3}$$

In equation (3), the product of PAR and HTN represents the effects of environmental resources on photosynthetic processes, and the product of FAPAR and Leaf Age indicates the section of photosynthesis related to canopy structure. We can therefore estimate the seasonal dynamic of availability of environmental resources and derive $DOY_{Resources}$.

$$\mathrm{Optimized\ GPP}_{max} = (\mathrm{FAPAR} \times \mathrm{Leaf\ Age})_{max} \times (\mathrm{PAR} \times \mathrm{HTN})_{max} \tag{4}$$

An optimized GPP_{max} would be achieved as the product of seasonal maximum canopy structure and environmental resources, assuming that plants could regulate the densest canopy structure to obtain the most abundant resources, namely adjusted DOY_{NDVI} equal to $DOY_{Resources}$.

Model simulations

We used GPP and LAI outputs from 14 DGVMs from the TRENDY S3 simulations (dynamic CO_2, climate and land use) to evaluate the performances of recent DGVMs to simulate peak vegetation growth[33]. These DGVMs included CABLE-POP, CLASS-CTEM, CLM5.0, DLEM, ISAM, JSBACH, JULES, LPJ-GUESS, LPX, OCN, ORCHIDEE, ORCHIDEE-CNP, SURFEX and VISIT (details of individual models in Supplementary Table 3). We retrieved annual peak timings of vegetation photosynthesis (DOY_{GPP}) and canopy structure (DOY_{LAI}) from 2000 to 2017 and calculated their difference ($\delta DOY_{GPP,LAI}$). Then we compared the results with observed DOY_{CSIF}, DOY_{NDVI} and $\delta DOY_{CSIF,NDVI}$, respectively (Figs. 5 and 6 and Supplementary Figs. 3–5). The model outputs from TRENDY S0-S2 simulations were also used in our study and were reported in the temporal analysis section. All model outputs were linearly interpolated to daily temporal resolution and aggregated to 0.5° spatial resolution.

Temporal analysis

To explore the temporal variation of the mismatch in peak timing between vegetation photosynthesis and canopy structure and its potential drivers, we first examined the trend in absolute $\delta DOY_{CSIF,NDVI}$ during 2000–2018, with positive and negative trends representing increasing and decreasing discrepancies between DOY_{CSIF} and DOY_{NDVI}, respectively (Fig. 6). Then, we identified potential drivers of the trend in $\delta DOY_{CSIF,NDVI}$ by developing a new BRT model considering temporal varying atmospheric CO_2 concentration and climatic variables. The new BRT model was initially built on the basis of the relationship of spatiotemporal variation between $\delta DOY_{CSIF,NDVI}$ and 19 explanatory variables, including varying atmospheric CO_2 concentration and 18 explanatory variables used in the spatial analysis. The effects of CO_2 fertilization and climate change on the trend in $\delta DOY_{CSIF,NDVI}$ can therefore be attributed based on the differences between the simulated results under varying CO_2 or climate and constant CO_2 or climate during 2000–2018 (Extended Data Fig. 4). Likewise, we estimated the contributions of CO_2 fertilization and climate change to the trend in absolute $\delta DOY_{GPP,LAI}$ based on the model outputs from the TRENDY S0-S2 simulations (Supplementary Fig. 6).

Reporting summary

Further information on research design is available in the Nature Portfolio Reporting Summary linked to this article.

Data availability

The CSIF dataset is from https://doi.org/10.17605/OSF.IO/8XQY6. The GOME-2 SIF dataset is from https://avdc.gsfc.nasa.gov/pub/data/satellite/MetOp/GOME_F/. The MODIS NDVI dataset is from https://lpdaac.usgs.gov/products/mod13c1v006/. The reprocessed LAI dataset is from http://globalchange.bnu.edu.cn/research/laiv6. The FLUXNET2015 dataset is from https://fluxnet.org/data/fluxnet2015-dataset/. The surface air temperature and Rad datasets are from https://rda.ucar.edu/datasets/ds314.3/. The SWC dataset is from https://disc.gsfc.nasa.gov/datasets/GLDAS_NOAH025_3H_2.1/summary?keywords=GLDAS. The SLA, Nm and Pm datasets are from https://github.com/abhirupdatta/global_maps_of_plant_traits. The canopy height and maximum rooting depth datasets are from https://webmap.ornl.gov/ogc/dataset.jsp?dg_id=10023_1 and https://wci.earth2observe.eu/thredds/catalog/usc/root-depth/catalog.html. The ASR and plant species datasets are from https://ecotope.org/anthromes/biodiversity/plants/data/ and https://databasin.org/datasets/43478f840ac84173979b22631c2ed672/. The tree density dataset is from https://elischolar.library.yale.edu/yale_fes_data/1/.

Code availability

All computer codes for the analysis of the data are available from the corresponding author on reasonable request.

References

1. Piao, S., Friedlingstein, P., Ciais, P., Viovy, N. & Demarty, J. Growing season extension and its impact on terrestrial carbon cycle in the Northern Hemisphere over the past 2 decades. *Glob. Biogeochem. Cycles* **21**, GB3018 (2007).
2. Richardson, A. D. et al. Climate change, phenology, and phenological control of vegetation feedbacks to the climate system. *Agric. For. Meteorol.* **169**, 156–173 (2013).
3. Xia, J., Niu, S., Ciais, P. & Janssens, I. A. Joint control of terrestrial gross primary productivity by plant phenology and physiology. *Proc. Natl Acad. Sci. USA* **112**, 2788–2793 (2015).
4. Yang, J. et al. Divergent shifts in peak photosynthesis timing of temperate and alpine grasslands in China. *Remote Sens. Environ.* **233**, 111395 (2019).
5. Huang, K., Xia, J., Wang, Y. & Ahlstrom, A. Enhanced peak growth of global vegetation and its key mechanisms. *Nat. Ecol. Evol.* **2**, 1897–1905 (2018).
6. Park, T., Chen, C. & Macias-Fauria, M. Changes in timing of seasonal peak photosynthetic activity in northern ecosystems. *Glob. Change Biol.* **25**, 2382–2395 (2019).
7. Medlyn, B. E. Physiological basis of the light use efficiency model. *Tree Physiol.* **18**, 167 (1998).
8. Turner, D. P., Urbanski, S., Bremer, D., Wofsy, S. C. & Gregory, M. A cross-biome comparison of daily light use efficiency for gross primary production. *Glob. Change Biol.* **9**, 383–395 (2003).
9. Monteith, J. L. Solar radiation and productivity in tropical ecosystems. *Appl. Ecol.* **9**, 747–766 (1972).
10. Wang, H. et al. Towards a universal model for carbon dioxide uptake by plants. *Nat. Plants* **3**, 734–741 (2017).
11. Zhang, Y., Joiner, J., Alemohammad, S. H., Zhou, S. & Gentine, P. A global spatially contiguous solar-induced fluorescence (CSIF) dataset using neural networks. *Biogeosciences* **15**, 5779–5800 (2018).
12. Frankenberg, C. et al. New global observations of the terrestrial carbon cycle from GOSAT: patterns of plant fluorescence with gross primary productivity. *Geophys. Res. Lett.* **38**, L17706 (2011).
13. Yuan, H., Dai, Y., Xiao, Z., Ji, D. & Shangguan, W. Reprocessing the MODIS Leaf Area Index products for land surface and climate modelling. *Remote Sens. Environ.* **115**, 1171–1187 (2011).
14. Elith, J., Leathwick, J. R. & Hastie, T. A working guide to boosted regression trees. *J. Anim. Ecol.* **77**, 802–813 (2008).
15. Wang, X. et al. Globally consistent patterns of asynchrony in vegetation phenology derived from optical, microwave, and fluorescence satellite data. *J. Geophys. Res. Biogeosci.* **125**, e2020JG005732 (2020).
16. Poorter, H. et al. Biomass allocation to leaves, stems and roots: meta-analyses of interspecific variation and environmental control. *New Phytol.* **193**, 30–50 (2012).
17. Zhang, Y., Commane, R., Zhou, S., Williams, A. P. & Gentine, P. Light limitation regulates the response of autumn terrestrial carbon uptake to warming. *Nat. Clim. Change* **10**, 739–743 (2020).
18. Yuan, W. et al. Global comparison of light use efficiency models for simulating terrestrial vegetation gross primary production based on the LaThuile database. *Agric. For. Meteorol.* **192-193**, 108–120 (2014).
19. Reich, P. B. et al. Temperature drives global patterns in forest biomass distribution in leaves, stems, and roots. *Proc. Natl Acad. Sci. USA* **111**, 13721–13726 (2014).
20. Wright, I. J., Reich, P. B. & Westoby, M. The worldwide leaf economics spectrum. *Nature* **428**, 821–827 (2004).
21. Reich, P. B., Oleksyn, J. & Wright, I. J. Leaf phosphorus influences the photosynthesis–nitrogen relation: a cross-biome analysis of 314 species. *Oecologia* **160**, 207–212 (2009).
22. Chen, Y., Han, W., Tang, L., Tang, Z. & Fang, J. Leaf nitrogen and phosphorus concentrations of woody plants differ in responses to climate, soil and plant growth form. *Ecography* **36**, 178–184 (2013).
23. Jiang, M., Caldararu, S., Zaehle, S., Ellsworth, D. S. & Medlyn, B. E. Towards a more physiological representation of vegetation phosphorus processes in land surface models. *New Phytol.* **222**, 1223–1229 (2019).
24. Kergoat, L., Lafont, S., Arneth, A., Le Dantec, V. & Saugier, B. Nitrogen controls plant canopy light-use efficiency in temperate and boreal ecosystems. *J. Geophys. Res. Biogeosci.* **113**, G04017 (2008).
25. Du, E. et al. Global patterns of terrestrial nitrogen and phosphorus limitation. *Nat. Geosci.* **13**, 221–226 (2020).
26. Cleveland, C. C. et al. Patterns of new versus recycled primary production in the terrestrial biosphere. *Proc. Natl Acad. Sci. USA* **110**, 12733–12737 (2013).
27. Veneklaas, E. J. et al. Opportunities for improving phosphorus-use efficiency in crop plants. *New Phytol.* **195**, 306–320 (2012).
28. Janssens, I. A. & Luyssaert, S. Nitrogen's carbon bonus. *Nat. Geosci.* **2**, 318–319 (2009).
29. Luo, X. et al. Global variation in the fraction of leaf nitrogen allocated to photosynthesis. *Nat. Commun.* **12**, 4866 (2021).
30. Lambers, H., Iii, F. & Pons, T. L. *Plant Physiological Ecology* (Springer, 2008).
31. Vose, J. M. et al. Factors influencing the amount and distribution of leaf area of pine stands. *Ecol. Bull.* **43**, 102–114 (1994).
32. Carter, S. K., Saenz, D. & Rudolf, V. H. W. Shifts in phenological distributions reshape interaction potential in natural communities. *Ecol. Lett.* **21**, 1143–1151 (2018).
33. Sitch, S. et al. Recent trends and drivers of regional sources and sinks of carbon dioxide. *Biogeosciences* **12**, 653–679 (2015).
34. Farquhar, G. D., von Caemmerer, S. & Berry, J. A. A biochemical model of photosynthetic CO_2 assimilation in leaves of C_3 species. *Planta* **149**, 78–90 (1980).
35. Krinner, G. et al. A dynamic global vegetation model for studies of the coupled atmosphere–biosphere system. *Glob. Biogeochem. Cycles* **19**, GB1015 (2005).
36. Murray-Tortarolo, G. et al. Evaluation of land surface models in reproducing satellite-derived LAI over the high-latitude Northern Hemisphere. Part I: Uncoupled DGVMs. *Remote Sens.* **5**, 4819–4838 (2013).

37. Lawrence, D. M. et al. The community land model version 5: description of new features, benchmarking, and impact of forcing uncertainty. *J. Adv. Model. Earth Syst.* **11**, 4245–4287 (2019).
38. Goll, D. S., Winkler, A. J. & Raddatz, T. Carbon–nitrogen interactions in idealized simulations with JSBACH (version 3.10). *Geosci. Model Dev.* **10**, 2009–2030 (2017).
39. Goll, D. S., Vuichard, N. & Maignan, F. A representation of the phosphorus cycle for ORCHIDEE (revision 4520). *Geosci. Model Dev.* **10**, 3745–3770 (2017).
40. Sun, Y., Goll, D. S. & Chang, J. Global evaluation of the nutrient-enabled version of the land surface model ORCHIDEE-CNP v1.2 (r5986). *Geosci. Model Dev.* **14**, 1987–2010 (2021).
41. Clark, D. B., Mercado, L. M. & Sitch, S. The Joint UK Land Environment Simulator (JULES), model description—Part 2: Carbon fluxes and vegetation dynamics. *Geosci. Model Dev.* **4**, 701–722 (2011).
42. Terrer, C. et al. Nitrogen and phosphorus constrain the CO_2 fertilization of global plant biomass. *Nat. Clim. Change* **9**, 684–689 (2019).
43. Reyes-Fox, M. et al. Elevated CO_2 further lengthens growing season under warming conditions. *Nature* **510**, 259–262 (2014).
44. Guanter, L. et al. Global and time-resolved monitoring of crop photosynthesis with chlorophyll fluorescence. *Proc. Natl Acad. Sci. USA* **111**, E1327–E1333 (2014).
45. Sun, Y. et al. OCO-2 advances photosynthesis observation from space via solar-induced chlorophyll fluorescence. *Science* **358**, eaam5747 (2017).
46. Joiner, J. et al. The seasonal cycle of satellite chlorophyll fluorescence observations and its relationship to vegetation phenology and ecosystem atmosphere carbon exchange. *Remote Sens. Environ.* **152**, 375–391 (2014).
47. Chu, D. et al. Long time-series NDVI reconstruction in cloud-prone regions via spatio-temporal tensor completion. *Remote Sens. Environ.* **264**, 112632 (2021).
48. Joiner, J. et al. Global monitoring of terrestrial chlorophyll fluorescence from moderate-spectral-resolution near-infrared satellite measurements: methodology, simulations, and application to GOME-2. *Atmos. Meas. Tech.* **6**, 2803–2823 (2013).
49. Zhang, Y., Joiner, J., Gentine, P. & Zhou, S. Reduced solar-induced chlorophyll fluorescence from GOME-2 during Amazon drought caused by dataset artifacts. *Glob. Change Biol.* **24**, 2229–2230 (2018).
50. Rodell, M., Houser, P. R. & Jambor, U. The Global Land Data Assimilation System. *Bull. Am. Meteorol. Soc.* **85**, 381–394 (2004).
51. Pastorello, G. et al. The FLUXNET2015 dataset and the ONEFlux processing pipeline for eddy covariance data. *Sci. Data* **7**, 225 (2020).
52. Reichstein, M. et al. On the separation of net ecosystem exchange into assimilation and ecosystem respiration: review and improved algorithm. *Glob. Change Biol.* **11**, 1424–1439 (2005).
53. LASSLOP, G. et al. Separation of net ecosystem exchange into assimilation and respiration using a light response curve approach: critical issues and global evaluation. *Glob. Change Biol.* **16**, 187–208 (2010).
54. Vautard, R., Yiou, P. & Ghil, M. Singular-spectrum analysis: a toolkit for short, noisy chaotic signals. *Phys. D.* **58**, 95–126 (1992).
55. Zhou, S. et al. Dominant role of plant physiology in trend and variability of gross primary productivity in North America. *Sci. Rep.* **7**, 41366 (2017).
56. Butler, E. E., Datta, A. & Flores-Moreno Mapping local and global variability in plant trait distributions. *Proc. Natl Acad. Sci. USA* **114**, E10937–E10946 (2017).
57. Simard, M., Pinto, N., Fisher, J. B. & Baccini, A. Mapping forest canopy height globally with spaceborne lidar. *J. Geophys. Res. Biogeosci.* **116**, G04021 (2011).
58. Ellis, E. C., Antill, E. C. & Kreft, H. All is not loss: plant biodiversity in the anthropocene. *PLoS ONE* **7**, e30535 (2012).
59. Kier, G., Mutke, J., Dinerstein, E., Ricketts, T. H. & Barthlott, W. Global patterns of plant diversity and floristic knowledge. *J. Biogeogr.* **32**, 1107–1116 (2005).
60. Boles, S. H. et al. Land cover characterization of temperate East Asia using multi-temporal VEGETATION sensor data. *Remote Sens. Environ.* **90**, 477–489 (2004).

Acknowledgements

This study was supported by the National Natural Science Foundation of China (41988101), the Second Tibetan Plateau Scientific Expedition and Research Program (grant no. 2019QZKK0208) and the Xplorer Prize. Z.Z. was supported by the National Natural Science Foundation of China (41901122) and the Shenzhen Fundamental Research Program (GXWD20201231165807007-20200814213435001). J.P. was supported by the Spanish Government grant PID2019-110521GB-I00, the Fundación Ramón Areces grant CIVP20A6621 and the Catalan Government grants SGR2017-1005 and AGAUR-2020PANDE00117. We thank H. Vallicrosa from CSIC, Global Ecology Unit CREAF-CSIC-UAB for discussion. We also thank I. MacLachlan from Peking University for proofreading. We are grateful for the computational resources provided by the High-performance Computing Platform of Peking University's supercomputing facility.

Author contributions

S.P. and Z.Z. designed the study. Q.Z. performed the analysis. Q.Z., S.P. and Z.Z. wrote the initial draft. All authors, including H.Z., R.M., Y.Z. and J.P., contributed to the interpretation of the results and the writing of the paper.

Competing interests

The authors declare no competing interests.

Additional information

Extended data is available for this paper at https://doi.org/10.1038/s41477-022-01278-9.

Supplementary information The online version contains supplementary material available at https://doi.org/10.1038/s41477-022-01278-9.

Correspondence and requests for materials should be addressed to Zaichun Zhu or Shilong Piao.

Peer review information *Nature Plants* thanks William Smith and Sujong Jeong for their contribution to the peer review of this work.

 https://doi.org/10.1038/s41477-022-01278-9

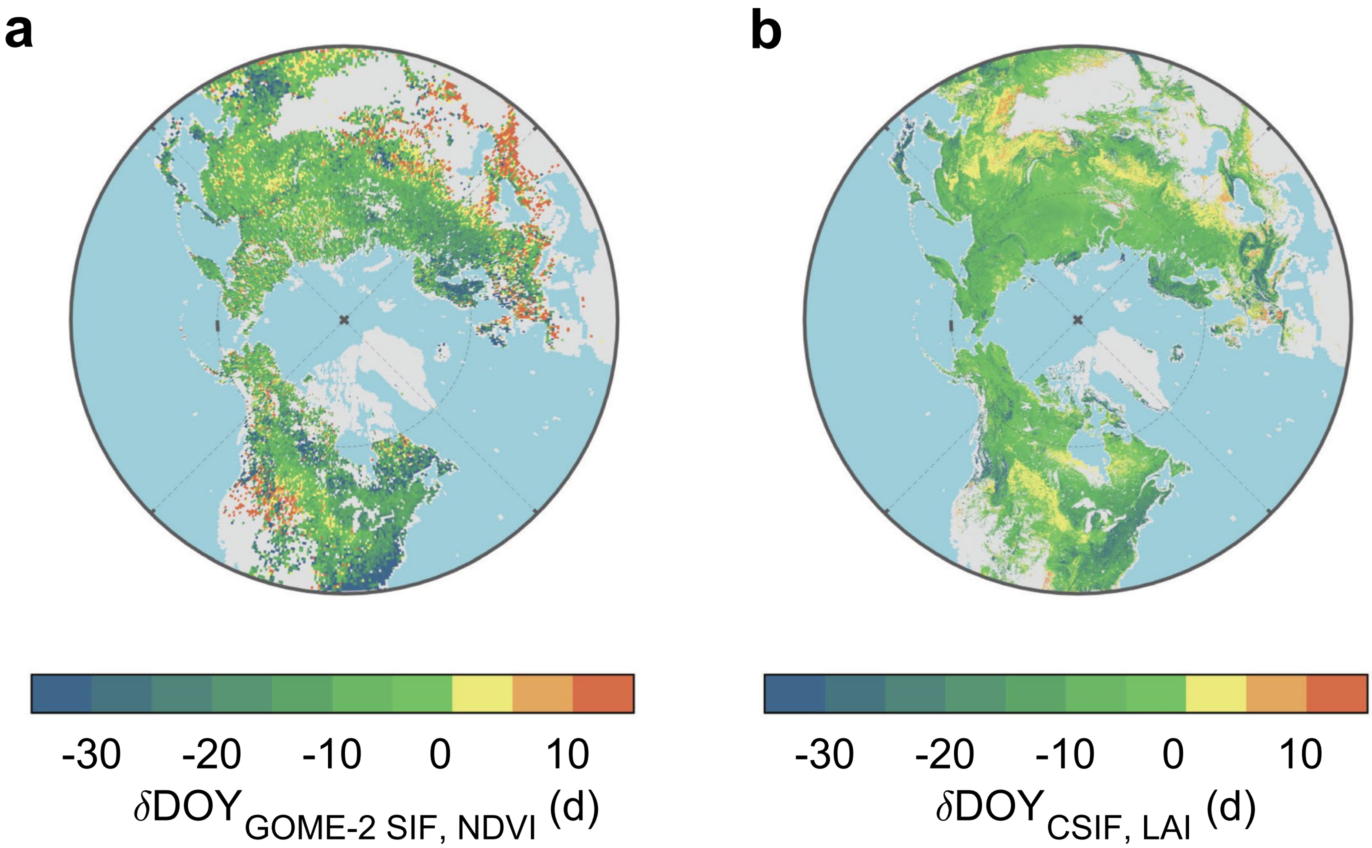

Extended Data Fig. 1 | Comparison between the timings of seasonal peak photosynthesis and canopy structure in northern ecosystems based on multiple proxies. Spatial patterns of the seasonal peak timing difference between photosynthesis and canopy structure represented by $\delta DOY_{GOME\text{-}2\ SIF,\ NDVI}$ (**a**) and $\delta DOY_{CSIF,\ LAI}$ (**b**).

https://doi.org/10.1038/s41477-022-01278-9

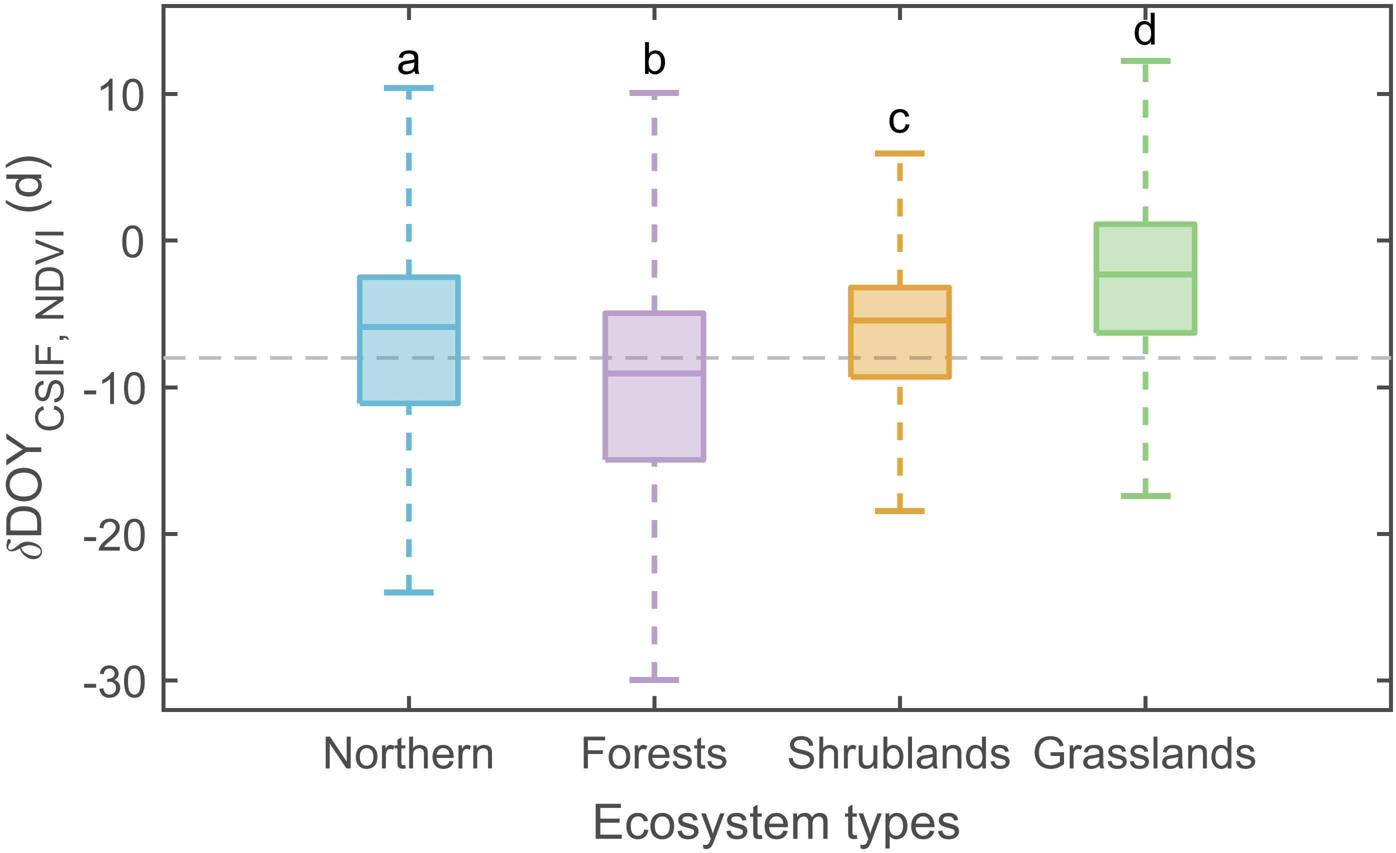

Extended Data Fig. 2 | Mean differences of seasonal peak timings between photosynthesis and canopy structure for different ecosystem types. Northern ecosystems ($n = 2578665$), forests ($n = 788343$), shrublands ($n = 765928$), and grasslands ($n = 344205$). Boxplots show the median, maximum, minimum, 25th, and 75th quartiles values (without outliers). The coloured letters represent significant differences (all p values $= 9.56 \times 10^{-10}$, two-sided Tukey's HSD test) in average $\delta DOY_{CSIF, NDVI}$ among ecosystems estimated by one-way analysis of variance (ANOVA).

https://doi.org/10.1038/s41477-022-01278-9

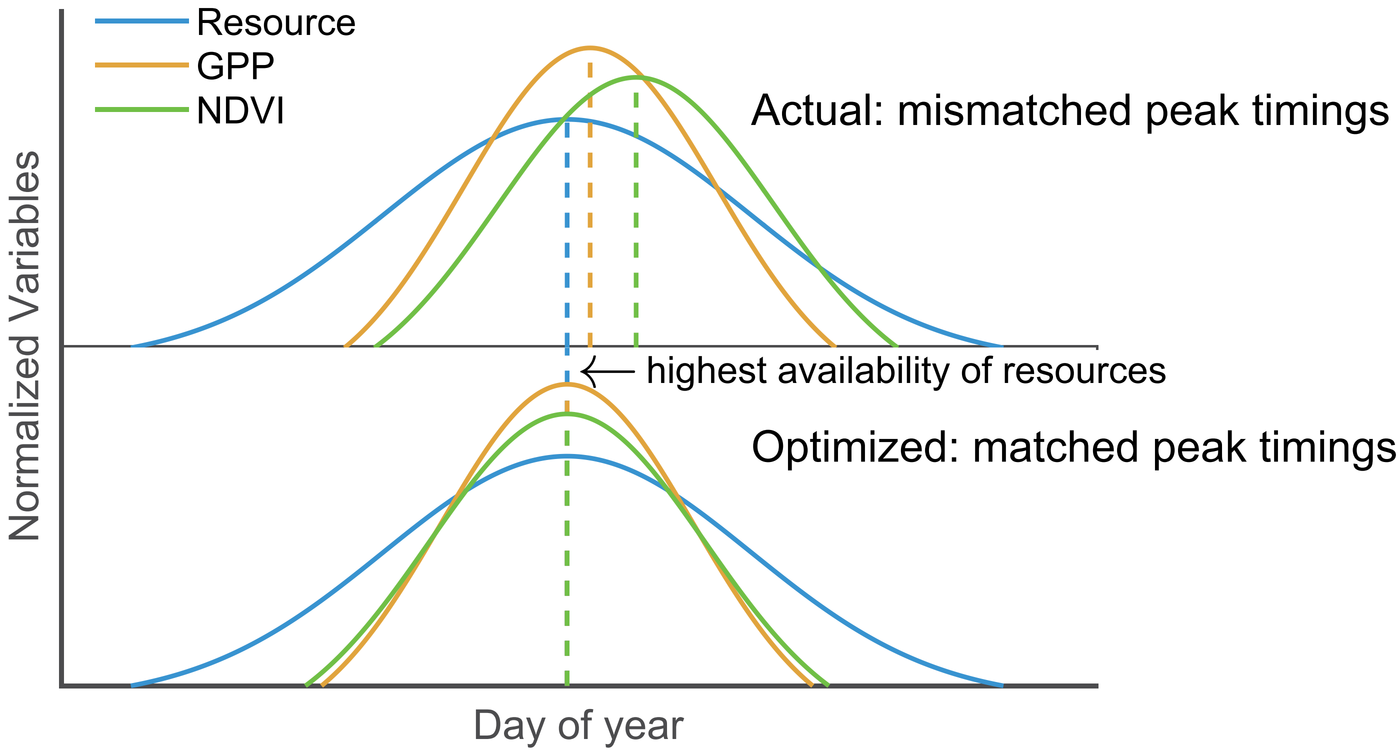

Extended Data Fig. 3 | Illustration of the optimal GPP_{max} conceptual model. Coloured curves indicate the seasonal cycles of environmental resources (Resource, blue), photosynthesis (GPP, orange), and canopy structure (NDVI, green). The seasonal peak timing of the canopy structure is adjusted to match the highest availability of environmental resources ($DOY_{NDVI} = DOY_{Resource}$), and therefore the optimized maximum seasonal GPP was achieved.

 https://doi.org/10.1038/s41477-022-01278-9

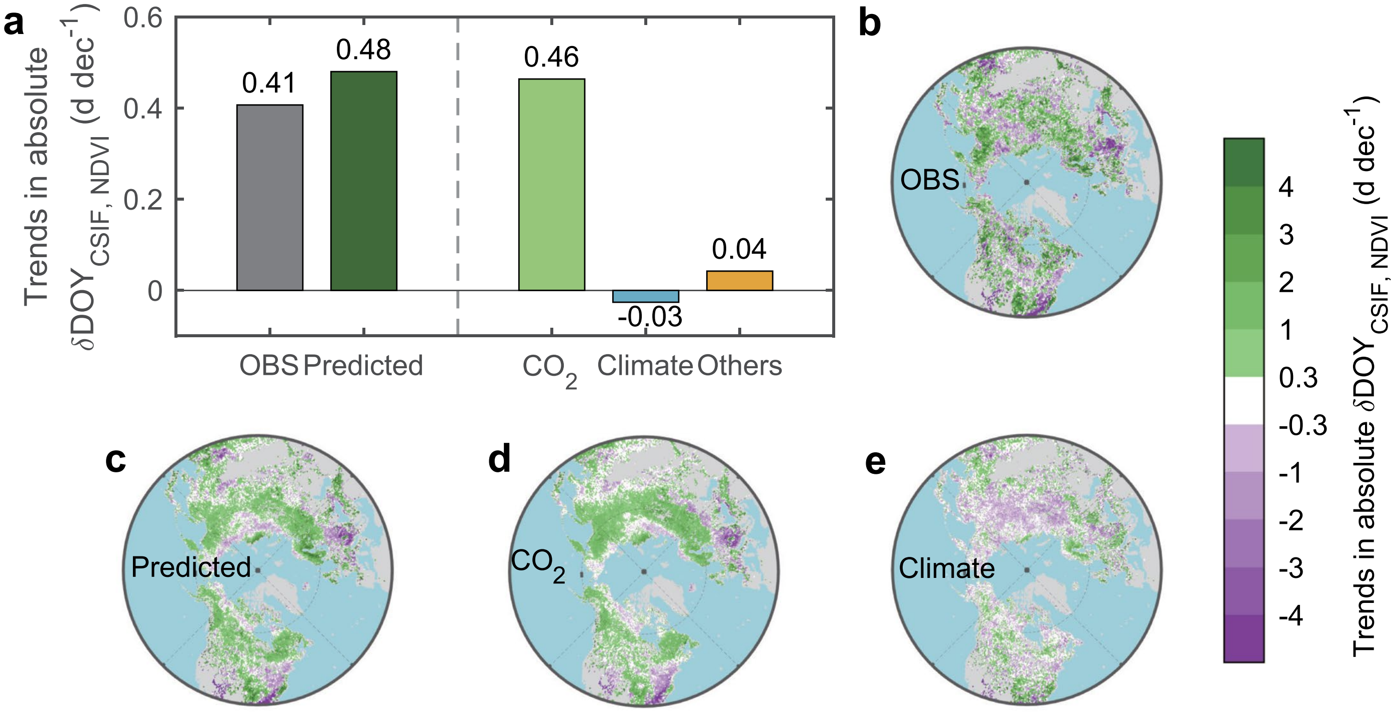

Extended Data Fig. 4 | Attribution of the trends in absolute $\delta DOY_{CSIF, NDVI}$ in northern ecosystems during 2000–2017. a, Trends in spatially averaged absolute $\delta DOY_{CSIF, NDVI}$ derived from satellite observation (OBS) and BRT models (Predicted), and attributed respectively to rising CO_2 (CO_2), climate change (Climate), and other factors (Others). **b-e**, Spatial patterns of the trends in absolute $\delta DOY_{CSIF, NDVI}$ corresponding to the columns in **a**. The satellite observation was resampled to 0.5° to match the spatial resolution of explanatory variables in the BRT model.

nature portfolio

Corresponding author(s): Shilong Piao
Zaichun Zhu

Last updated by author(s): Oct 11, 2022

Reporting Summary

Nature Portfolio wishes to improve the reproducibility of the work that we publish. This form provides structure for consistency and transparency in reporting. For further information on Nature Portfolio policies, see our Editorial Policies and the Editorial Policy Checklist.

Statistics

For all statistical analyses, confirm that the following items are present in the figure legend, table legend, main text, or Methods section.

n/a	Confirmed	
☐	☒	The exact sample size (*n*) for each experimental group/condition, given as a discrete number and unit of measurement
☒	☐	A statement on whether measurements were taken from distinct samples or whether the same sample was measured repeatedly
☐	☒	The statistical test(s) used AND whether they are one- or two-sided *Only common tests should be described solely by name; describe more complex techniques in the Methods section.*
☐	☒	A description of all covariates tested
☐	☒	A description of any assumptions or corrections, such as tests of normality and adjustment for multiple comparisons
☐	☒	A full description of the statistical parameters including central tendency (e.g. means) or other basic estimates (e.g. regression coefficient) AND variation (e.g. standard deviation) or associated estimates of uncertainty (e.g. confidence intervals)
☐	☒	For null hypothesis testing, the test statistic (e.g. *F*, *t*, *r*) with confidence intervals, effect sizes, degrees of freedom and *P* value noted *Give P values as exact values whenever suitable.*
☒	☐	For Bayesian analysis, information on the choice of priors and Markov chain Monte Carlo settings
☐	☒	For hierarchical and complex designs, identification of the appropriate level for tests and full reporting of outcomes
☒	☐	Estimates of effect sizes (e.g. Cohen's *d*, Pearson's *r*), indicating how they were calculated

Our web collection on statistics for biologists contains articles on many of the points above.

Software and code

Policy information about availability of computer code

Data collection	No software was used to collect data. All datasets are downloaded from the original sources.
Data analysis	The analyses and mapping were both performed using MATLAB (R2019b). Machine-learning algorithm, the boosted regression trees (BRT) models were fitted in R (4.1.0) with extending 'gbm' library. All codes used in this study can be provided by the corresponding author upon reasonable requests.

For manuscripts utilizing custom algorithms or software that are central to the research but not yet described in published literature, software must be made available to editors and reviewers. We strongly encourage code deposition in a community repository (e.g. GitHub). See the Nature Portfolio guidelines for submitting code & software for further information.

Data

Policy information about availability of data

All manuscripts must include a data availability statement. This statement should provide the following information, where applicable:

- Accession codes, unique identifiers, or web links for publicly available datasets
- A description of any restrictions on data availability
- For clinical datasets or third party data, please ensure that the statement adheres to our policy

All data used in this study are publicly accessible. The CSIF data set is from https://doi.org/10.17605/OSF.IO/8XQY6, the GOME-2 SIF data set is from https://avdc.gsfc.nasa.gov/pub/data/satellite/MetOp/GOME_F/, the MODIS NDVI data set is from https://lpdaac.usgs.gov/products/mod13c1v006/, the reprocessed LAI data set is from http://globalchange.bnu.edu.cn/research/laiv6, the FLUXNET2015 data set is from https://fluxnet.org/data/fluxnet2015-dataset/, the surface air temperature and shortwave radiation data sets are from https://rda.ucar.edu/datasets/ds314.3/, the soil-water content data set is from https://disc.gsfc.nasa.gov/datasets/GLDAS_NOAH025_3H_2.1/summary?keywords=GLDAS, the SLA, Nm, and Pm data sets are from https://github.com/abhirupdatta/

global_maps_of_plant_traits, the canopy height and maximum rooting depth data sets are from https://webmap.ornl.gov/ogc/dataset.jsp?dg_id=10023_1 and https://wci.earth2observe.eu/thredds/catalog/usc/root-depth/catalog.html, the ASR and plant species data sets are from https://ecotope.org/anthromes/biodiversity/plants/data/ and https://databasin.org/datasets/43478f840ac84173979b22631c2ed672/ and the tree density data set is from https://elischolar.library.yale.edu/yale_fes_data/1/.

Field-specific reporting

Please select the one below that is the best fit for your research. If you are not sure, read the appropriate sections before making your selection.

☐ Life sciences ☐ Behavioural & social sciences ☒ Ecological, evolutionary & environmental sciences

For a reference copy of the document with all sections, see nature.com/documents/nr-reporting-summary-flat.pdf

Ecological, evolutionary & environmental sciences study design

All studies must disclose on these points even when the disclosure is negative.

Study description	We reported a prevalent and increasing mismatch between the timing of maximum seasonal photosynthesis and canopy structure in the northern lands (>30°N) and investigated the responsible factors for this mismatch using a mix of observations and models.
Research sample	The satellite-observed data sets of SIF (CSIF and GOME-2 SIF) and vegetation indices (NDVI and LAI), and climate data sets were used to derive the timing of seasonal photosynthesis, canopy structure, and climatic factors. The eddy-covariance Gross Primary Productivity data were from FLUXNET data sets. 52 individual FLUXNET sites were used in this study. Details were reported in the Method section.
Sampling strategy	We only considered the satellite-observed pixels and flux-tower sites where vegetation only have one seasonal peak during the growing season from summer to autumn.
Data collection	All data sets were download from the URLs in the data availability statement in the main text.
Timing and spatial scale	The CSIF data set has 4-d temporal and 0.05° spatial resolutions. The GOME-2 SIF data set has daily temporal and 40km×40km spatial resolutions. The NDVI data set has 16-d temporal and 0.05° spatial resolutions. The LAI data set has 8-d temporal and 0.05° spatial resolutions. The surface air temperature and shortwave radiation data sets from CRU-NCEP have 6-h temporal and 0.5° spatial resolutions. The soil-water content data set from GLDAS has 3-h temporal and 0.25° spatial resolutions. The predictive variables in the BRT models were obtained from original resolutions and aggregated into a common spatial resolution of 0.5°. Details were reported in the Method section.
Data exclusions	We excluded the satellite-observed pixels and flux-tower sites where vegetation have multiple seasonal peaks using a harmonic analysis. We also ignored the vegetation areas with low seasonality based on a threshold of the coefficient of variation of annual NDVI.
Reproducibility	Our analyses were based on public satellite and climate products and well-defined methods, and the results could be reliably reproduced.
Randomization	When we analyzed the underlying mechanisms of the mismatch between the peak timings of NDVI and CSIF for each vegetation types, we allocated the vegetated pixels into different groups according to the vegetation type information derived from the MODIS land cover map.
Blinding	Not applicable. The data used in this study have specific temporal and spatial information.

Did the study involve field work? ☐ Yes ☒ No

Reporting for specific materials, systems and methods

We require information from authors about some types of materials, experimental systems and methods used in many studies. Here, indicate whether each material, system or method listed is relevant to your study. If you are not sure if a list item applies to your research, read the appropriate section before selecting a response.

Materials & experimental systems

n/a	Involved in the study	
☒	☐	Antibodies
☒	☐	Eukaryotic cell lines
☒	☐	Palaeontology and archaeology
☒	☐	Animals and other organisms
☒	☐	Human research participants
☒	☐	Clinical data
☒	☐	Dual use research of concern

Methods

n/a	Involved in the study	
☒	☐	ChIP-seq
☒	☐	Flow cytometry
☒	☐	MRI-based neuroimaging